PERGAMON

International Journal of Solids and Structures 40 (2003) 4879–4894

INTERNATIONAL JOURNAL OF SOLIDS and STRUCTURES

www.elsevier.com/locate/ijsolstr

On the estimation of K_t at a bottom of a grind-out cavity after one-sided patching

C.N. Duong *

The Boeing Company, 5301 Bolsa Avenue, MC H013-A316, Huntington Beach, CA 92647-2099, USA

Received 8 July 2002

Abstract

An unsupported plate containing an embedded grind-out cavity repaired with a reinforcement bonded on one side may experience a considerable out-of-plane bending near a cavity due to the load-path eccentricity even when the geometrically nonlinear effect is taken into account. This out-of-plane bending causes stresses in the plate near the bottom of the cavity vary significantly through a remaining plate's thickness with inner wall fiber stresses in some cases at 20–30% higher than the corresponding plane-stress type results, i.e., those without considering the out-of-plane deflections. A plane-stress type analysis of a repair over a corrosion cavity had been presented in a previous paper by Duong et al. [Theoretical and Applied Fracture Mechanics 36 (2001a) 187] for a constant depth cavity repaired with an elliptical patch and most recently by Duong and Yu [International Journal of Engineering Science 40 (2002a) 347] for a spherical depth cavity repaired with a polygonal patch. Extension of these methods to include the effect of out-of-plane bending therefore will be delineated in the present paper.

Keywords: Stress concentration; Composite repairs; Corrosion repairs; Eigenstrain; Eigencurvature; Grind-out cavity

1. Introduction

Corrosion damage on the outer surfaces of aircraft is generally removed by grinding during periodic, routine maintenance. Aircraft manufacturers provide maintenance specifications that allow a limited amount of material removal, but it is sometimes necessary to exceed these limits in order to completely remove the corrosion. In these cases, the structure must be replaced or repaired before further operation of the aircraft is permitted. Whenever a repair is sought, bonded composite doublers may be preferred due to high stiffness and high strength of the composite.

In the past, stress analysis of a bonded repair over a corrosion grind-out cavity was normally done using the finite element method. The corrosion repairs are thought to be too complex to be analyzed by an analytical method. However, the authors in the recent papers presented a two-stage analysis procedure for

* Tel.: +1-714-896-6204; fax: +1-714-896-6505.
E-mail address: cong.n.duong@boeing.com (C.N. Duong).

0020-7683/03/$ - see front matter © 2003 Published by Elsevier Ltd.
doi:10.1016/S0020-7683(03)00218-X

analyzing this repair problem analytically (Duong et al., 2001a; Duong and Yu, 2002a). This procedure followed Rose's original approach (1988) for the analysis of crack patching and it accounted for various complexities such as polygon-shaped patch, a grind-out cavity with a spherical depth, and the effects of thermal stresses due to curing and/or cruising. The procedure had been used successfully in estimating stresses and strains in a patch and skin at various critical locations such as near the patch edge, around a grind-out, and at a bottom of a grind-out cavity. However, all previous analytical analyses had been limited to a case of plane stress.

Although a symmetrical repair is the most effective reinforcement, unsymmetrical repairs provide a clear advantage when it is difficult or not possible to access both sides of a structure. In this case, unless the structure is well supported against the out-of-plane deflection, for example by stiffeners attached to one side of the structure, the out-of-plane bending due to the load path eccentricity causes stresses in the repaired skin near the bottom of the grind-out cavity vary significantly through a remaining skin's thickness with inner wall fiber stresses in some cases at 20–30% higher than the corresponding plane-stress type results (i.e., those without considering the out-of-plane deflections). This necessitates an analysis of out-of-plane bending in an unsupported bonded corrosion repair.

In this paper, an approximate analytical method based on a hybrid global–local approach is introduced to solve for a large deflection problem of a bonded plate with an embedded cavity under thermo-mechanical loading. For simplicity, the bonded plate is assumed to be under a uniform temperature change and the patch is rigidly bonded to the plate whenever it is in direct contact with the plate. This rigid bond assumption ignores the finite width of the load transfer zone around the boundary of the reinforcement, which is valid when the actual width of the load transfer zone is small relative to the in-plane dimensions of the reinforcement. Since analytical solutions for polygon-shaped inclusions with uniform and quadratic eigenstrains (Rodin, 1996; Duong et al., 2001b) and with uniform eigencurvature (Duong and Yu, 2002b) are available, it is more convenient to solve the present bonded plate problem using the equivalent inclusion method (Beom and Earmme, 1999; Mura, 1987).

2. Problem statements and analytical approach

Consider an infinite isotropic plate containing an embedded spherical depth grind-out cavity of an elliptical shape and repaired with a polygon-shaped reinforcement Ω (see Fig. 1). Both reinforcement and cavity assume to be symmetric with respect to the global coordinate axes. The reinforcement is either isotropic or orthotropic with its material principal axes parallel to x_1 and x_2 axes. Let us further assume that the reinforcement when it is orthotropic will have a larger mismatch in the thermal expansion coefficient with the base plate along the x_2-direction. The bonded plate is subjected to a uniform temperature change ΔT and also uniform strains or stresses at infinity. When uniform stresses are prescribed at infinity, one can simply convert them to strains using Hook's law. For simplicity, all shear components are assumed to be zero. The objective here is to obtain the inner wall fiber stresses at the bottom of a grind-out cavity after patching. It is rather unwieldy to solve the stated problem using a rigorous geometrically nonlinear analysis. We will therefore present here an approximate solution based on a hybrid global–local approach as that employed by Wang and Rose (1999) for crack patching. This approach is proposed in details below and results obtained from the proposed approach will be compared with 3-D FE solutions.

The problem stated above will be solved in three steps, each with a different set of assumptions and simplifications as follows (see Fig. 2):

Step 1—Global analysis: In the global analysis, by ignoring the grind-out cavity embedded in the infinite isotropic plate and considering the large deflection, the global strains and curvatures at the prospective damage location can be determined. These strains and curvatures will be later used as far field boundary

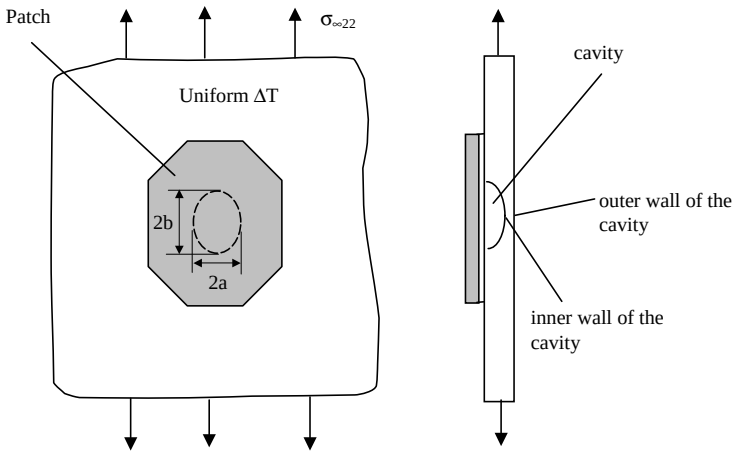

Fig. 1. Geometry of a composite bonded repair over a grind-out cavity.

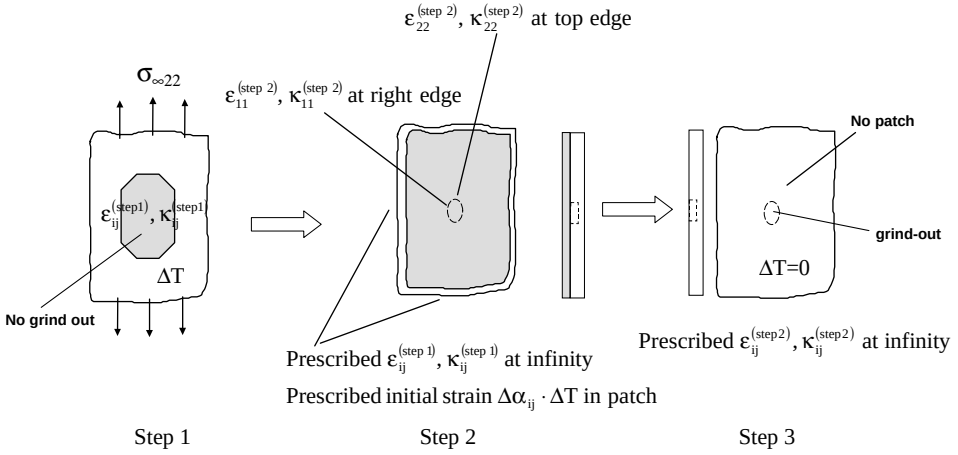

Fig. 2. Three steps of the proposed analysis procedure.

conditions for a local analysis where the effect of the grind-out cavity is accounted for (Duong et al., 2001a; Duong and Yu, 2002a).

The local analysis of the grind-out problem will be carried out using a similar approach by Hart-Smith (2002) for computing peel and shear stresses in the adhesive of the single sided patched plate. That approach will be explained as follows. By expressing the transverse displacements of the plate and patch as

$$\begin{aligned} w_{\mathrm{p}} &= \tfrac{1}{2}(w_{\mathrm{p}} + w_{\mathrm{R}}) + \tfrac{1}{2}(w_{\mathrm{p}} - w_{\mathrm{R}}) \\ w_{\mathrm{R}} &= \tfrac{1}{2}(w_{\mathrm{p}} + w_{\mathrm{R}}) - \tfrac{1}{2}(w_{\mathrm{p}} - w_{\mathrm{R}}) \end{aligned} \tag{1}$$

where the subscripts 'p' and 'R' denote the plate and reinforcement (patch), respectively, Hart-Smith (2002) assumed that these transverse displacements could be obtained by adding the results from two separated analyses. In the first analysis, the average transverse displacement of the patch–plate combination is

determined approximately from the rigid bond analysis. The transverse displacement in the plate in that case will be also that of the patch–plate combination because of the rigid bond assumption and it represents only one part of the total transverse displacement of the plate. On the hand, to account for the relative displacement between the plate and patch due to the existence of a thin adhesive layer between them, a second analysis is performed to determine the relative displacement $(w_p - w_R)$ with results from the former analysis imposed as boundary conditions. By denoting w_I as the transverse displacement of the patch–plate combination obtained from the Hart-Smith first analysis, the final transverse displacement of the plate is given by

$$w_p = w_I + \tfrac{1}{2}(w_p - w_R) \tag{2}$$

From the above equation, it is worthy to note that the transverse displacement of the plate obtained from the Hart-Smith first analysis contributes 100% of its value to the final displacement of the plate while the relative displacement $(w_p - w_R)$ obtained from the second analysis has only half of its value contributed to the final displacement. In a similar manner, the bending stresses at the bottom of the grind-out cavity will also be determined from two separated analyses corresponding to steps 2 and 3 below.

Step 2: In step 2, the patch is assumed to be infinite, *isotropic*, and an integral part of the isotropic plate and the plate contains an elliptical grind-out cavity. Step 2 then involves solving a problem of an infinite patched plate containing an embedded elliptical grind-out cavity under far field strains and curvatures obtained from step 1. This step will be performed within the framework of geometrically linear elasticity. The main objectives of step 2 analysis are (i) to determine the outer wall fiber stress, thus the bending stress, at the bottom of the grind out cavity (after patching), associated with the unison deflection of the patch–plate combination, and (ii) to derive the local strains and curvatures near the edges of the grind-out cavity for use in step 3 below, assuming that these strains and curvature are only different from the global strains and curvatures by small perturbations. Step 2 analysis will provide the bending stress at the bottom of the grind-out cavity in the average sense in the same spirit as the Hart-Smith first analysis of the single sided patched plate for w_I. Since the wall of the cavity tends to deflect toward the patch, the outer wall fiber stress at the bottom of the cavity will be lower than the corresponding plane stress result (the one without considering the out-of-plane deflection). The average bending stress at the bottom of the cavity will be estimated from this step as

$$\sigma_0^{b(\text{step }2)} \approx \sigma_{22}^{p(\text{plane-stress})}(\mathbf{0}) - \sigma_{22(\text{outer-wall})}^{p(\text{step }2)}(\mathbf{0}) \tag{3}$$

where the center of the cavity is located at point **0**. It should be emphasized that the corresponding plane stress solution $\sigma_{22}^{p(\text{plane-stress})}(\mathbf{0})$ is available and given earlier by Duong and Yu (2002a). For a cavity either filled with a typical adhesive or unfilled, the patch and the base plate deform differently inside the grind-out region. Thus, the result of the maximum through thickness stress, i.e., the inner wall fiber stress, at the bottom of the cavity obtained from step 2 will not be sufficiently accurate for the repair assessment. In the same spirit as the Hart-Smith second analysis of the single sided patched plate, a step 3 analysis is therefore required for the present corrosion repair problem to account for the fact that the deflections of the patch and plate are relatively independent inside the cavity. Since practically no load transfer will take place between the plate and the patch inside the cavity, stresses in the plate at the bottom of the grind-out cavity will be governed solely by the plate's stresses at the edge of the grind-out. In other words, if the plate's stresses at the edges of the grind-out are known, the plate's stresses at the bottom of the cavity can be determined from these edge's stresses from another separate analysis without considering the patch. This explains why the patch is not modeled in step 3 below.

Step 3: In step 3, an un-patched plate with an embedded grind-out cavity is considered, with the strains and curvatures obtained from step 2 at the edges of the grind-out applied at infinity. The analysis is again performed within the framework of geometrically linear elasticity. The objective of step 3 is to determine

the bending stress at the bottom of the cavity when the plate and patch deflect quite independently inside the cavity. This bending stress is defined as $\frac{1}{2}(\sigma^{\mathrm{p(step\,3)}}_{22(\text{inner-wall})}(\mathbf{0}) - \sigma^{\mathrm{p(step\,3)}}_{22(\text{outer-wall})}(\mathbf{0}))$. Since the plate's strains and curvatures obtained from step 2 at the edge of the grind-out cavity are imposed in the present un-patched plate problem at infinity, the average-thickness stress (or mean stress) at the bottom of the cavity of the problem considered in this step may be different from those of the originally sought problem. The bending stress obtained from this step therefore will also be scaled with respect to the corresponding plane stress result according to the following:

$$\sigma_0^{\mathrm{b(step\,3)}} = \frac{\left(\sigma^{\mathrm{p(step\,3)}}_{22(\text{inner-wall})}(\mathbf{0}) - \sigma^{\mathrm{p(step\,3)}}_{22(\text{outer-wall})}(\mathbf{0})\right)}{\left(\sigma^{\mathrm{p(step\,3)}}_{22(\text{inner-wall})}(\mathbf{0}) + \sigma^{\mathrm{p(step\,3)}}_{22(\text{outer-wall})}(\mathbf{0})\right)}\sigma_{22}^{\mathrm{p(plane\text{-}stress)}}(\mathbf{0}) \tag{4}$$

In light of Eq. (2), the total bending stress at the bottom of the cavity finally can be expressed as

$$\sigma_0^{\mathrm{b}} = \sigma_0^{\mathrm{b(step\,2)}} + \tfrac{1}{2}\sigma_0^{\mathrm{b(step\,3)}} \tag{5}$$

where $\sigma_0^{\mathrm{b(step\,3)}}$ and $\sigma_0^{\mathrm{b(step\,3)}}$ are previously defined via Eqs. (3) and (4). The maximum stress at the bottom of the grind-out cavity will be at the inner wall, which is given by

$$\sigma_{22}^{\max}(\mathbf{0}) = \sigma_{22}^{\mathrm{p(plane\text{-}stress)}}(\mathbf{0}) + \sigma_0^{\mathrm{b}} = \sigma_{22}^{\mathrm{p(plane\text{-}stress)}}(\mathbf{0}) + \sigma_0^{\mathrm{b(step\,2)}} + \tfrac{1}{2}\sigma_0^{\mathrm{b(step\,3)}} \tag{6}$$

It remains now to outline a solution method for each step of the above procedure and that will be the topic of the next section.

3. Solution method

Solution methods for the above three steps will be delineated here. The solution method for step 1 was given in an earlier paper by the authors in Duong and Yu (2002c). The description of the solution method for step 1 therefore will be omitted from this paper. Nevertheless, to better understand the present hybrid local–global approach, key results presented in the cited reference will be discussed here and the reader should refer to that reference for further details. It was shown in Duong and Yu (2002c) that the neutral plane of the reinforced region tended to align exactly with the load line for the remote tensile load, thus reducing the bending moment in the middle of the reinforced plate or at the prospective damage location. For a combination of relatively high patch's length to the plate's thickness ratio and a relatively high remote tensile load, this alignment is closed to perfect, resulting in little or no bending moment in the middle of the reinforced plate. In that case, step 1 can be solved approximately under plane stress assumption. Another significant result found in the cited reference is that the alignment of the neutral plane with the load line for the tensile load occurs at a lower load level when the thermal loads are present, providing that a same patch configuration has been considered in both loading cases with and without thermal effects. Since most of the corrosion repairs are evaluated at a relatively high tensile load corresponding to either the design limit load (DLL) or the design ultimate load (DUL) and with thermal effects, the bending moments at the prospective damage location in these repairs in many cases are practically zero. In those cases, a plane stress analysis will be sufficient for step 1 and such plane stress solution is available in Duong et al. (2001b).

We now devote our effort to outline the solution methods for steps 2 and 3 of the hybrid local–global approach. The solution method for step 2 will be delineated first in Section 3.1.

3.1. Solution method for step 2 analysis

3.1.1. Formulation

For clarity, a description of the problem analyzed in step 2 will be repeated here in details. Let us consider an infinite bi-material (fully patched) isotropic plate containing an embedded elliptical grind-out cavity over domain $\Re$ as illustrated in Fig. 2(b). The reader is reminded that the patch in step 2's analysis assumes to be infinite and isotropic. The extensional, coupling and bending stiffness A^0_{ijkl}, B^0_{ijkl}, D^0_{ijkl} of the bi-material plate are defined according to a classical laminate theory as (Jones, 1975):

$$\begin{aligned} A^0_{ijkl} &= \int_0^{t_p} C^p_{ijkl}\,dz + \int_{t_p}^{t_p+t_R} C^R_{ijkl}\,dz \\ B^0_{ijkl} &= \int_0^{t_p} C^p_{ijkl}(z-h_0)\,dz + \int_{t_p}^{t_p+t_R} C^R_{ijkl}(z-h_0)\,dz \\ D^0_{ijkl} &= \int_0^{t_p} C^p_{ijkl}(z-h_0)^2\,dz + \int_{t_p}^{t_p+t_R} C^R_{ijkl}(z-h_0)^2\,dz \end{aligned} \tag{7}$$

where h_0 is the z-coordinate of the neutral plane measured from the lower surface of the bi-material plate and it can be found from a condition $B^0_{22}=0$; C_{ijkl} is the elasticity tensor; t is the thickness; the superscripts or subscripts 'p', 'R', '0' denote the repaired plate, the reinforcement, and the bi-material plate, respectively. C^R_{ijkl} is calculated based on the assumption that the patch is isotropic with a modulus and Poisson ratio equal to the principal modulus E_{22} and ν_{12}, respectively.

Follow the work of Duong and Yu (2002a), the thickness profile of a base (repaired) plate inside the cavity region $\Re$ is approximated by

$$t_{\text{p-inside}}(x_1,x_2) = t_r + \frac{1}{2R_c}\left(x_1^2 + \frac{x_2^2}{\beta^2}\right) \tag{8}$$

where t_r is the minimum remaining plate thickness inside $\Re$, β is an aspect ratio of the elliptical cavity, and R_c is a geometric parameter defined in Fig. 3. It should be noted that for a circular grind-out cavity ($\beta=1$), Eq. (8) implies that the plate thickness profile in the cavity is axisymmetric. For simplicity, the patch and the plate inside region $\Re$ assume to deform as if they are connected by a series of rigid shear springs and rigid extensional springs with the axial direction of the extensional spring parallel to a normal vector of the repaired plate. Any deficiency resulting from this rather restricted assumption is remedied by using the

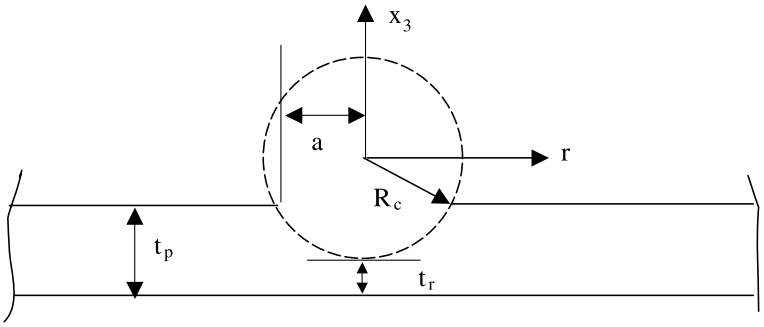

Fig. 3. Detailed geometry of a cross section of a plate containing a spherical deep grind-out cavity. In the figure, "a" is minor axis of the elliptical grind-out as shown in Fig. 1.

approach outlined in Section 2. The region $\Re$ thus can be treated as an inhomgeneity of a bi-material plate with extensional, coupling and bending stiffness tensors given by

$$\begin{aligned} A^{\mathrm{I}}_{ijkl} &= \int_0^{t_{\text{p-inside}}} C^{\mathrm{p}}_{ijkl}\,\mathrm{d}z + \int_{t_{\mathrm{p}}}^{t_{\mathrm{p}}+t_{\mathrm{R}}} C^{\mathrm{R}}_{ijkl}\,\mathrm{d}z \\ B^{\mathrm{I}}_{ijkl} &= \int_0^{t_{\text{p-inside}}} C^{\mathrm{p}}_{ijkl}(z-h_0)\,\mathrm{d}z + \int_{t_{\mathrm{p}}}^{t_{\mathrm{p}}+t_{\mathrm{R}}} C^{\mathrm{R}}_{ijkl}(z-h_0)\,\mathrm{d}z \\ D^{\mathrm{I}}_{ijkl} &= \int_0^{t_{\text{p-inside}}} C^{\mathrm{p}}_{ijkl}(z-h_0)^2\,\mathrm{d}z + \int_{t_{\mathrm{p}}}^{t_{\mathrm{p}}+t_{\mathrm{R}}} C^{\mathrm{R}}_{ijkl}(z-h_0)^2\,\mathrm{d}z \end{aligned} \tag{9}$$

In the above equation, h_0 is the z-coordinate of a neutral plane of the bi-material plate (thus of the region outside $\Re$), t_{p} is the full thickness of the repaired plate, and $t_{\text{p-inside}}$ is given by Eq. (8). Also, it should be noted that in Eq. (9) the upper limit of the first integral of the right hand side (t_{p}) is different from the lower limit of the second integral ($t_{\text{p-inside}}$) since the patch is not in direct contact with the repaired plate in $\Re$ due to the presence of the cavity (Fig. 1).

The fully patched plate is subjected to a strain field $\varepsilon_{\infty ij}$ and curvature field $\kappa_{\infty ij}$ at infinity. $\varepsilon_{\infty ij}$ and $\kappa_{\infty ij}$ are related respectively to the strains and curvatures obtained from step 1 at the middle of the reinforced plate by

$$\varepsilon_{\infty ij} = \varepsilon^{(\text{step 1})}_{ij}\Big|_{\text{plate's middle}} + \left(h_0 - \frac{t_{\mathrm{p}}}{2}\right)\kappa^{(\text{step 1})}_{ij}\Big|_{\text{plate's middle}} \tag{10}$$

$$\kappa_{\infty ij} = \kappa^{(\text{step 1})}_{ij}\Big|_{\text{plate's middle}} \tag{11}$$

Since the reference plane at which the main plane strains are measured is chosen at $z = t_{\mathrm{p}}/2$ in step 1 while it is at the neutral plane of the bi-material plate in step 2, such different choice of the reference plane therefore must be taken into account in the present formulation. That explains the relationship given in Eq. (10). It should be noted that if step 1 is obtained from a plane stress analysis as mentioned in Section 2, tensor $\kappa_{\infty ij}$ is then equal to zero. In addition to the above far field strain and curvature, as derived in Duong and Yu (2002a), the reinforcement layer of the bi-material plate is prescribed by the following uniform initial strain field associated with the thermal expansion mismatch between the patch and the plate:

$$\varepsilon^{(\mathrm{T})(\mathrm{R})}_{ij} = \Delta\alpha_{ij}\Delta T \tag{12}$$

where $\Delta\alpha_{ij} = (\alpha^{\mathrm{R}}_{ij} - \alpha^{\mathrm{p}}_{ij})$, α_{ij} is thermal expansion coefficient tensor, and ΔT is the uniform temperature change. That initial strain field induces the following thermal force and thermal moment per unit width, which applied to all regions of the bi-material plate, both inside and outside $\Re$ (Jones, 1975):

$$\begin{aligned} N^{(\mathrm{T})}_{ij} &= t_{\mathrm{R}} C^{\mathrm{R}}_{ijkl}\varepsilon^{(\mathrm{T})(\mathrm{R})}_{kl} \\ M^{(\mathrm{T})}_{ij} &= \chi_1 C^{\mathrm{R}}_{ijkl}\varepsilon^{(\mathrm{T})(\mathrm{R})}_{kl} \end{aligned} \tag{13}$$

where

$$\chi_1 = \frac{(t_{\mathrm{p}} + t_{\mathrm{R}} - h_0)^2 - (t_{\mathrm{p}} - h_0)^2}{2} \tag{14}$$

Again, if the solution of step 1 is obtained from a plane stress analysis, χ_1 will be assumed to be zero in this step for consistency. With the analyzing problem completely stated, we are now ready to outline its solution method. We begin the development with a brief summary of the constitutive relations for the inhomogeneous region $\Re$ and the surrounding region as given below:

- For an inhomogeneity $\Re$

$$\begin{aligned} N_{ij}^{\mathrm{I}} &= A_{ijkl}^{\mathrm{I}}\left(\bar{\varepsilon}_{kl}^{\mathrm{I}} + \varepsilon_{\infty kl}\right) + B_{ijkl}^{\mathrm{I}}\left(\kappa_{kl}^{\mathrm{I}} + \kappa_{\infty kl}\right) - N_{ij}^{(\mathrm{T})} \\ M_{ij}^{\mathrm{I}} &= B_{ijkl}^{\mathrm{I}}\left(\bar{\varepsilon}_{kl}^{\mathrm{I}} + \varepsilon_{\infty kl}\right) + D_{ijkl}^{\mathrm{I}}\left(\kappa_{kl}^{\mathrm{I}} + \kappa_{\infty kl}\right) - M_{ij}^{(\mathrm{T})} \end{aligned} \tag{15}$$

- For a region outside $\Re$

$$\begin{aligned} N_{ij}^{0} &= A_{ijkl}^{0}\left(\bar{\varepsilon}_{kl}^{0} + \varepsilon_{\infty kl}\right) + B_{ijkl}^{0}\left(\kappa_{kl}^{0} + \kappa_{\infty kl}\right) - N_{ij}^{(\mathrm{T})} \\ M_{ij}^{0} &= B_{ijkl}^{0}\left(\bar{\varepsilon}_{kl}^{0} + \varepsilon_{\infty kl}\right) + D_{ijkl}^{0}\left(\kappa_{kl}^{0} + \kappa_{\infty kl}\right) - M_{ij}^{(\mathrm{T})} \end{aligned} \tag{16}$$

Here N_{ij} and M_{ij} are the stress and moment resultant defined as $N_{ij} = \int_0^t \sigma_{ij}\,\mathrm{d}z$ and $M_{ij} = \int_0^t \sigma_{ij}(z - h_0)\,\mathrm{d}z$. $\bar{\varepsilon}_{ij}$ and κ_{ij} are the incremental main plane strain and curvature due the presence of the inhomogeneity and due to the thermal force and moment. They are defined as $\bar{\varepsilon}_{ij} = \frac{1}{2}(u_{i,j} + u_{j,i})$ and $\kappa_{ij} = -(\partial^2 w/\partial x_i \partial x_j)$, where u_i and w are incremental main plane displacements and incremental transverse displacement, respectively. Next we want to show that the present problem with the prescribed thermal force and moment above can be formulated as an inhomogeneity problem with its own eigenstrain and eigencurvature. This class of problem is well studied in micromechanics. It involves an infinite domain of homogeneous material D containing a finite subdomain $\Re$ of a different material with inelastic strain (eigenstrain) and inelastic curvature (eigencurvature) fields prescribed in $\Re$ and these fields are zero in region D–$\Re$.

By defining $\varepsilon_{ij}^{(\mathrm{init})(0)}$, $\kappa_{ij}^{(\mathrm{init})(0)}$, $\varepsilon_{ij}^{(\mathrm{init})(\mathrm{I})}$ and $\kappa_{ij}^{(\mathrm{init})(\mathrm{I})}$ as,

$$\begin{Bmatrix} \varepsilon_{ij}^{(\mathrm{init})(0)} \\ \kappa_{ij}^{(\mathrm{init})(0)} \end{Bmatrix} = \begin{bmatrix} A_{ijkl}^{0} & B_{ijkl}^{0} \\ B_{ijkl}^{0} & D_{ijkl}^{0} \end{bmatrix}^{-1} \begin{Bmatrix} N_{kl}^{(\mathrm{T})} \\ M_{kl}^{(\mathrm{T})} \end{Bmatrix} \tag{17}$$

$$\begin{Bmatrix} \varepsilon_{ij}^{(\mathrm{init})(\mathrm{I})} \\ \kappa_{ij}^{(\mathrm{init})(\mathrm{I})} \end{Bmatrix} = \begin{bmatrix} A_{ijkl}^{\mathrm{I}} & B_{ijkl}^{\mathrm{I}} \\ B_{ijkl}^{\mathrm{I}} & D_{ijkl}^{\mathrm{I}} \end{bmatrix}^{-1} \begin{Bmatrix} N_{kl}^{(\mathrm{T})} \\ M_{kl}^{(\mathrm{T})} \end{Bmatrix} \tag{18}$$

it is then very easy to show that Eqs. (15) and (16) can be rewritten as

$$\begin{aligned} N_{ij}^{\mathrm{I}} &= A_{ijkl}^{\mathrm{I}}\left[\bar{\varepsilon}_{kl}^{\mathrm{I}} + \varepsilon_{\infty kl} - \varepsilon_{kl}^{(\mathrm{init})(0)} - \left(\varepsilon_{kl}^{(\mathrm{init})(\mathrm{I})} - \varepsilon_{kl}^{(\mathrm{init})(0)}\right)\right] + B_{ijkl}^{\mathrm{I}}\left[\kappa_{kl}^{\mathrm{I}} + \kappa_{\infty kl} - \kappa_{kl}^{(\mathrm{init})(0)} - \left(\kappa_{kl}^{(\mathrm{init})(\mathrm{I})} - \kappa_{kl}^{(\mathrm{init})(0)}\right)\right] \\ M_{ij}^{\mathrm{I}} &= B_{ijkl}^{\mathrm{I}}\left[\bar{\varepsilon}_{kl}^{\mathrm{I}} + \varepsilon_{\infty kl} - \varepsilon_{kl}^{(\mathrm{init})(0)} - \left(\varepsilon_{kl}^{(\mathrm{init})(\mathrm{I})} - \varepsilon_{kl}^{(\mathrm{init})(0)}\right)\right] + D_{ijkl}^{\mathrm{I}}\left[\kappa_{kl}^{\mathrm{I}} + \kappa_{\infty kl} - \kappa_{kl}^{(\mathrm{init})(0)} - \left(\kappa_{kl}^{(\mathrm{init})(\mathrm{I})} - \kappa_{kl}^{(\mathrm{init})(0)}\right)\right] \end{aligned} \tag{19}$$

for $\mathbf{x} \in \Re$, and

$$\begin{aligned} N_{ij}^{0} &= A_{ijkl}^{0}\left(\bar{\varepsilon}_{kl}^{0} + \varepsilon_{\infty kl} - \varepsilon_{kl}^{(\mathrm{init})(0)}\right) + B_{ijkl}^{0}\left(\kappa_{kl}^{0} + \kappa_{\infty kl} - \kappa_{kl}^{(\mathrm{init})(0)}\right) \\ M_{ij}^{0} &= B_{ijkl}^{0}\left(\bar{\varepsilon}_{kl}^{0} + \varepsilon_{\infty kl} - \varepsilon_{kl}^{(\mathrm{init})(0)}\right) + D_{ijkl}^{0}\left(\kappa_{kl}^{0} + \kappa_{\infty kl} - \kappa_{kl}^{(\mathrm{init})(0)}\right) \end{aligned} \tag{20}$$

for $\mathbf{x} \in D$–$\Re$. From Eqs. (19) and (20), it is clear that $\left(\varepsilon_{ij}^{(\mathrm{init})(\mathrm{I})} - \varepsilon_{ij}^{(\mathrm{init})(0)}\right)$ and $\left(\kappa_{ij}^{(\mathrm{init})(\mathrm{I})} - \kappa_{ij}^{(\mathrm{init})(0)}\right)$ are the eigenstrain and eigencurvature of the inhomogeneity since they are prescribed in $\Re$ and vanish in D–$\Re$, thus, what remains now is to solve for the elastic solution of an infinite plate of a homogeneous material with stiffnesses given by Eq. (7), containing an inhomogeneity $\Re$ of a different material with stiffnesses given by Eq. (9), subjected to a uniform strain and curvature field $\left(\varepsilon_{\infty ij} - \varepsilon_{ij}^{(\mathrm{init})(0)}\right)$ and $\left(\kappa_{\infty ij} - \kappa_{ij}^{(\mathrm{init})(0)}\right)$ at infinity, and prescribed with an eigenstrain and eigencurvature field $\left(\varepsilon_{ij}^{(\mathrm{init})(\mathrm{I})} - \varepsilon_{ij}^{(\mathrm{init})(0)}\right)$ and $\left(\kappa_{ij}^{(\mathrm{init})(\mathrm{I})} - \kappa_{ij}^{(\mathrm{init})(0)}\right)$ inside $\Re$, using the equivalent inclusion method.

3.1.2. Equivalent inclusion method

In the equivalent inclusion method, the stress, main plane strain and curvature fields induced by an inhomogeneity occupied region $\Re$ will be the same as those induced by eigenstrain field ε^*_{ij} and eigencurvature field κ^*_{ij} in the same region of a homogeneous material when ε^*_{ij} and κ^*_{ij} are selected appropriately. The latter homogeneous problem is called an inclusion problem with the constitutive relation given by

$$\left\{ \begin{array}{c} N^{\mathrm{H}}_{ij} \\ M^{\mathrm{H}}_{ij} \end{array} \right\} = \left\{ \begin{array}{l} A^0_{ijkl}\left(\bar{\varepsilon}^{\mathrm{H}}_{kl} + \varepsilon_{\infty kl} - \varepsilon^{(\mathrm{init})(0)}_{kl} - \varepsilon^*_{kl}\right) + B^0_{ijkl}\left(\kappa^{\mathrm{H}}_{kl} + \kappa_{\infty kl} - \kappa^{(\mathrm{init})(0)}_{kl}\right) \\ B^0_{ijkl}\left(\bar{\varepsilon}^{\mathrm{H}}_{kl} + \varepsilon_{\infty kl} - \varepsilon^{(\mathrm{init})(0)}_{kl}\right) + D^0_{ijkl}\left(\kappa^{\mathrm{H}}_{kl} + \kappa_{\infty kl} - \kappa^{(\mathrm{init})(0)}_{kl} - \kappa^*_{kl}\right) \end{array} \right\} \tag{21}$$

for $\mathbf{x} \in \Re$, and

$$\left\{ \begin{array}{c} N^{\mathrm{H}}_{ij} \\ M^{\mathrm{H}}_{ij} \end{array} \right\} = \left\{ \begin{array}{l} A^0_{ijkl}\left(\bar{\varepsilon}^{\mathrm{H}}_{kl} + \varepsilon_{\infty kl} - \varepsilon^{(\mathrm{init})(0)}_{kl}\right) + B^0_{ijkl}\left(\kappa^{\mathrm{H}}_{kl} + \kappa_{\infty kl} - \kappa^{(\mathrm{init})(0)}_{kl}\right) \\ B^0_{ijkl}\left(\bar{\varepsilon}^{\mathrm{H}}_{kl} + \varepsilon_{\infty kl} - \varepsilon^{(\mathrm{init})(0)}_{kl}\right) + D^0_{ijkl}\left(\kappa^{\mathrm{H}}_{kl} + \kappa_{\infty kl} - \kappa^{(\mathrm{init})(0)}_{kl}\right) \end{array} \right\} \tag{22}$$

for $\mathbf{x} \in D$–$\Re$. In the above equation, the superscript H denotes the homogeneous problem. For a given ε^*_{ij} and κ^*_{ij}, solutions of the homogeneous (inclusion) problem exist. For ε^*_{ij} given as a second ordered polynomial of the position coordinate axes, i.e.,

$$\varepsilon^*_{ij} = F_{ij} + F_{ijkl}x_k x_l \tag{23}$$

it was shown in Duong et al. (2001b) that the elastic solution for the main plane strain field can be expressed as

$$\bar{\varepsilon}^{\mathrm{H}}_{ij} = S_{ijkl}F_{kl} + S_{ijklmn}F_{klmn} \tag{24}$$

where F_{ij} and F_{ijkl} are constant tensors, S_{ijkl} and S_{ijklmn} are called Eshelby tensors. These Eshelby tensors can be evaluated for any polygon-shaped inclusion using the algorithmic approach outlined in Rodin (1996) and Duong et al. (2001b). These detailed evaluations will be omitted here for reason of space. Similarly, for a given constant (or uniform) κ^*_{ij} field, the elastic solution for the curvature field is given by

$$\kappa^{\mathrm{H}}_{ij} = K_{ijkl}R_{kl} \tag{25}$$

$$\kappa^*_{ij} = R_{ij} \tag{26}$$

where R_{ij} is a constant tensor, K_{ijkl} is a Eshelby-type tensor for curvature transformation. The detailed evaluation of K_{ijkl} for a polygonal inclusion is presented in Duong and Yu (2002b) and again it will be omitted here. S_{ijkl}, S_{ijklmn} and K_{ijkl} in general are functions of spatial coordinates for points inside and outside region $\Re$. It should be emphasized that since the main-plane displacements u_i and the transverse displacement w do not depend on the coupling stiffness and are identical for the problem of a symmetric laminate with the same stiffness A^0_{ijkl} and D^0_{ijkl} (Beom and Earmme, 1999), the elastic solutions for the main plane strain and curvature field of the homogeneous problem can be obtained independently as suggested by Eqs. (24) and (25).

The present inhomogeneity problem may appear to be the same as that considered earlier by Beom and Earmme (1999). However, it is different since the stiffness tensors of the inhomogeneity in the present problem are not constant in $\Re$. This is because the thickness of the repaired plate varies inside $\Re$ according to the profile given by Eq. (8). As a result, it may require the use of high ordered polynomials for ε^*_{ij} and κ^*_{ij} in the analysis. However, to simplify the analysis, the present inhomogeneity problem will be solved using a quadratic eigenstrain and a constant eigencurvature theory. In addition, the stiffness tensors of the inhomogeneity given by Eq. (9) will be approximated by

$$
\begin{aligned}
&A^{\mathrm{I}}_{ijkl} = A^{\mathrm{I(min)}}_{ijkl} + \frac{t_{\mathrm{p}}}{2R_{\mathrm{c}}}\left(x_1^2 + \frac{x_2^2}{\beta^2}\right)C^{\mathrm{p}}_{ijkl} = A^{\mathrm{I(min)}}_{ijkl} + \left(x_1^2 + \frac{x_2^2}{\beta^2}\right)A^{(\mathrm{prime})}_{ijkl}\\
&A^{(\mathrm{prime})}_{ijkl} = \frac{t_{\mathrm{p}}}{2R_{\mathrm{c}}}C^{\mathrm{p}}_{ijkl}\\
&B^{\mathrm{I}}_{ijkl} \approx B^{\mathrm{I(min)}}_{ijkl}\\
&D^{\mathrm{I}}_{ijkl} \approx D^{\mathrm{I(min)}}_{ijkl},
\end{aligned}
\tag{27}
$$

where $A^{\mathrm{I(min)}}_{ijkl}$, $B^{\mathrm{I(min)}}_{ijkl}$ and $D^{\mathrm{I(min)}}_{ijkl}$ are stiffness tensors of the inhomogeneity when $t_{\text{p-inside}}$ in Eq. (9) takes on a minimum thickness value, i.e., t_{r}.

As found in Duong and Yu (2002a), it is more convenient to use in the formulation a new initial strain and curvature field $\varepsilon^{(\mathrm{init})(\text{I-min})}_{ij}$ and $\kappa^{(\mathrm{init})(\text{I-min})}_{ij}$ defined as

$$
\begin{Bmatrix} \varepsilon^{(\mathrm{init})(\text{I-min})}_{ij} \\ \kappa^{(\mathrm{init})(\text{I-min})}_{ij} \end{Bmatrix} = \begin{bmatrix} A^{\mathrm{I(min)}}_{ijkl} & B^{\mathrm{I(min)}}_{ijkl} \\ B^{\mathrm{I(min)}}_{ijkl} & D^{\mathrm{I(min)}}_{ijkl} \end{bmatrix}^{-1} \begin{Bmatrix} N^{(\mathrm{T})}_{kl} \\ M^{(\mathrm{T})}_{kl} \end{Bmatrix}. \tag{28}
$$

From Eqs. (12) and (22), it is clear that $\varepsilon^{(\mathrm{init})(\text{I-min})}_{ij}$ and $\kappa^{(\mathrm{init})(\text{I-min})}_{ij}$ are related to $\varepsilon^{(\mathrm{init})(\mathrm{I})}_{ij}$ and $\kappa^{(\mathrm{init})(\mathrm{I})}_{ij}$ by

$$
\begin{bmatrix} A^{\mathrm{I(min)}}_{ijkl} & B^{\mathrm{I(min)}}_{ijkl} \\ B^{\mathrm{I(min)}}_{ijkl} & D^{\mathrm{I(min)}}_{ijkl} \end{bmatrix} \begin{Bmatrix} \varepsilon^{(\mathrm{init})(\text{I-min})}_{ij} \\ \kappa^{(\mathrm{init})(\text{I-min})}_{ij} \end{Bmatrix} = \begin{bmatrix} A^{\mathrm{I}}_{ijkl} & B^{\mathrm{I}}_{ijkl} \\ B^{\mathrm{I}}_{ijkl} & D^{\mathrm{I}}_{ijkl} \end{bmatrix} \begin{Bmatrix} \varepsilon^{(\mathrm{init})(\mathrm{I})}_{ij} \\ \kappa^{(\mathrm{init})(\mathrm{I})}_{ij} \end{Bmatrix} \tag{29}
$$

The use of this relation will greatly simplify the latter derivation.

Following a procedure similar to that given in Duong and Yu (2002a), by approximating ε^{*}_{ij} and κ^{*}_{ij} respectively by Eqs. (23) and (26) with F_{ij}, F_{ijkl} and R_{ij} are yet to be determined coefficients, and by expanding the elastic solutions for the resulting strain and curvature field of a homogeneous problem into a Taylor series, the equivalency condition requires that F_{ij}, F_{ijkl} and R_{ij} must satisfy the following system of linear equation (without summation on subscript α):

$$
\begin{aligned}
&\Delta A_{\alpha\alpha 11}L_{11}(\mathbf{0}) + \Delta A_{\alpha\alpha 22}L_{22}(\mathbf{0}) + A^{0}_{\alpha\alpha 11}F_{11} + A^{0}_{\alpha\alpha 22}F_{22} + \Delta B_{\alpha\alpha 11}P_{11}(\mathbf{0}) + \Delta B_{\alpha\alpha 22}P_{22}(\mathbf{0})\\
&\quad = -\Delta A_{\alpha\alpha 11}\left(\varepsilon_{\infty 11} - \varepsilon^{(\mathrm{init})(0)}_{11}\right) - \Delta A_{\alpha\alpha 22}\left(\varepsilon_{\infty 22} - \varepsilon^{(\mathrm{init})(0)}_{22}\right) + A^{\mathrm{I(min)}}_{\alpha\alpha 11}\left(\varepsilon^{(\mathrm{init})(\text{I-min})}_{11} - \varepsilon^{(\mathrm{init})(0)}_{11}\right)\\
&\qquad + A^{\mathrm{I(min)}}_{\alpha\alpha 22}\left(\varepsilon^{(\mathrm{init})(\text{I-min})}_{22} - \varepsilon^{(\mathrm{init})(0)}_{22}\right) - \Delta B_{\alpha\alpha 11}\left(\kappa_{\infty 11} - \kappa^{(\mathrm{init})(0)}_{11}\right) - \Delta B_{\alpha\alpha 22}\left(\kappa_{\infty 22} - \kappa^{(\mathrm{init})(0)}_{22}\right)\\
&\qquad + B^{\mathrm{I(min)}}_{\alpha\alpha 11}\left(\kappa^{(\mathrm{init})(\text{I-min})}_{11} - \kappa^{(\mathrm{init})(0)}_{11}\right) + B^{\mathrm{I(min)}}_{\alpha\alpha 22}\left(\kappa^{(\mathrm{init})(\text{I-min})}_{22} - \kappa^{(\mathrm{init})(0)}_{22}\right)\\
&\frac{1}{2}\Delta A_{\alpha\alpha 11}\frac{\partial^2}{\partial x_1^2}L_{11}(\mathbf{0}) + \frac{1}{2}\Delta A_{\alpha\alpha 22}\frac{\partial^2}{\partial x_1^2}L_{22}(\mathbf{0}) + A^{0}_{\alpha\alpha 11}F_{1111} + A^{0}_{\alpha\alpha 22}F_{2211} + A^{(\mathrm{prime})}_{\alpha\alpha 11}L_{11}(\mathbf{0}) + A^{(\mathrm{prime})}_{\alpha\alpha 22}L_{22}(\mathbf{0})\\
&\quad + \frac{1}{2}\Delta B_{\alpha\alpha 11}\frac{\partial^2}{\partial x_1^2}P_{11}(\mathbf{0}) + \frac{1}{2}\Delta B_{\alpha\alpha 22}\frac{\partial^2}{\partial x_1^2}P_{22}(\mathbf{0}) = -A^{(\mathrm{prime})}_{\alpha\alpha 11}\varepsilon_{\infty 11} - A^{(\mathrm{prime})}_{\alpha\alpha 22}\varepsilon_{\infty 22}\\
&\frac{1}{2}\Delta A_{\alpha\alpha 11}\frac{\partial^2}{\partial x_2^2}L_{11}(\mathbf{0}) + \frac{1}{2}\Delta A_{\alpha\alpha 22}\frac{\partial^2}{\partial x_2^2}L_{22}(\mathbf{0}) + A^{0}_{\alpha\alpha 11}F_{1122} + A^{0}_{\alpha\alpha 22}F_{2222} + \frac{1}{\beta^2}A^{(\mathrm{prime})}_{\alpha\alpha 11}L_{11}(\mathbf{0}) + \frac{1}{\beta^2}A^{(\mathrm{prime})}_{\alpha\alpha 22}L_{22}(\mathbf{0})\\
&\quad + \frac{1}{2}\Delta B_{\alpha\alpha 11}\frac{\partial^2}{\partial x_2^2}P_{11}(\mathbf{0}) + \frac{1}{2}\Delta B_{\alpha\alpha 22}\frac{\partial^2}{\partial x_2^2}P_{22}(\mathbf{0}) = -\frac{1}{\beta^2}A^{(\mathrm{prime})}_{\alpha\alpha 11}\varepsilon_{\infty 11} - \frac{1}{\beta^2}A^{(\mathrm{prime})}_{\alpha\alpha 22}\varepsilon_{\infty 22}\\
&\Delta B_{\alpha\alpha 11}L_{11}(\mathbf{0}) + \Delta B_{\alpha\alpha 22}L_{22}(\mathbf{0}) + \Delta D_{\alpha\alpha 11}P_{11}(\mathbf{0}) + \Delta D_{\alpha\alpha 22}P_{22}(\mathbf{0}) + D^{0}_{\alpha\alpha 11}R_{11} + D^{0}_{\alpha\alpha 22}R_{22}\\
&\quad = -\Delta B_{\alpha\alpha 11}\left(\varepsilon_{\infty 11} - \varepsilon^{(\mathrm{init})(0)}_{11}\right) - \Delta B_{\alpha\alpha 22}\left(\varepsilon_{\infty 22} - \varepsilon^{(\mathrm{init})(0)}_{22}\right) - \Delta D_{\alpha\alpha 11}\left(\kappa_{\infty 11} - \kappa^{(\mathrm{init})(0)}_{11}\right)\\
&\qquad - \Delta D_{\alpha\alpha 22}\left(\kappa_{\infty 22} - \kappa^{(\mathrm{init})(0)}_{22}\right) + B^{\mathrm{I(min)}}_{\alpha\alpha 11}\left(\varepsilon^{(\mathrm{init})(\text{I-min})}_{11} - \varepsilon^{(\mathrm{init})(0)}_{11}\right) + B^{\mathrm{I(min)}}_{\alpha\alpha 22}\left(\varepsilon^{(\mathrm{init})(\text{I-min})}_{22} - \varepsilon^{(\mathrm{init})(0)}_{22}\right)\\
&\qquad + D^{\mathrm{I(min)}}_{\alpha\alpha 11}\left(\kappa^{(\mathrm{init})(\text{I-min})}_{11} - \kappa^{(\mathrm{init})(0)}_{11}\right) + D^{\mathrm{I(min)}}_{\alpha\alpha 22}\left(\kappa^{(\mathrm{init})(\text{I-min})}_{22} - \kappa^{(\mathrm{init})(0)}_{22}\right)
\end{aligned}
\tag{30}
$$

where

$$\begin{aligned}
\Delta A_{ijkl} &= A^{\mathrm{I(min)}}_{ijkl} - A^{0}_{ijkl} \\
\Delta B_{ijkl} &= B^{\mathrm{I(min)}}_{ijkl} - B^{0}_{ijkl} \\
\Delta D_{ijkl} &= D^{\mathrm{I(min)}}_{ijkl} - D^{0}_{ijkl} \\
L_{\alpha\beta}(\mathbf{x}) &= S_{\alpha\beta 11}(\mathbf{x})F_{11} + S_{\alpha\beta 22}(\mathbf{x})F_{22} + S_{\alpha\beta 1111}(\mathbf{x})F_{1111} + S_{\alpha\beta 1122}(\mathbf{x})F_{1122} + S_{\alpha\beta 2211}(\mathbf{x})F_{2211} + S_{\alpha\beta 2222}(\mathbf{x})F_{2222} \\
P_{\alpha\beta}(\mathbf{x}) &= K_{\alpha\beta 11}(\mathbf{x})R_{11} + K_{\alpha\beta 22}(\mathbf{x})R_{22} \quad (\alpha,\beta = 1,2)
\end{aligned} \tag{31}$$

the notation $L_{\alpha\beta}(\mathbf{0})$, etc. means that $L_{\alpha\beta}(\mathbf{0})$ being evaluated at point (0, 0), the origin of the coordinate system. Eq. (30) involves evaluations of the second derivatives of the Eshelby tensors and Eshelby-type tensors (via $(\partial^2/\partial x_j^2)L_{\alpha\beta}(\mathbf{x})$ and $(\partial^2/\partial x_j^2)P_{\alpha\beta}(\mathbf{x})$) and these computations can be carried out using an algorithm outlined in Duong et al. (2001b). It should be noted that Eq. (30) had been derived by (i) equating Eq. (21) of the homogeneous problem to Eq. (19) of the inhomogeneous problem with the stiffness tensors of the inhomogeneity approximated by Eq. (27), (ii) invoking the relation (29), and (iii) imposing conditions $\varepsilon^{\mathrm{I}}_{ij} = \varepsilon^{\mathrm{H}}_{ij}$ and $\kappa^{\mathrm{I}}_{ij} = \kappa^{\mathrm{H}}_{ij}$. In addition, results from Eqs. (24) and (25) for $\bar{\varepsilon}^{\mathrm{H}}_{ij}$ and κ^{H}_{ij} had also been utilized in the derivation with $\bar{\varepsilon}^{\mathrm{H}}_{ij}$ and κ^{H}_{ij} each being expanded into a Taylor series and retaining up to a second ordered term of the series.

It should be emphasized that the only unknowns in Eq. (30) are the coefficients F_{ij}, F_{ijkl} and R_{ij} of the assumed eigenstrain and eigencurvature field. Once these unknown coefficients are determined by solving Eq. (30), the main plane strain $\bar{\varepsilon}^{\mathrm{H}}_{ij}$ and curvature κ^{H}_{ij} of the homogeneous problem can be calculated via Eqs. (24) and (25). The corresponding stress and moment resultants N^{H}_{ij} and M^{H}_{ij} then can be evaluated using Eqs. (21) and (22). The stresses in the base plate and in the patch are finally given by

$$\begin{aligned}
\sigma^{\mathrm{p}}_{ij} &= C^{\mathrm{p}}_{ijkl}\left(\varepsilon^{\mathrm{I}}_{kl} + \varepsilon_{\infty kl} + (z-h_0)\left(\kappa^{\mathrm{I}}_{kl} - \kappa_{\infty kl}\right)\right) \\
\sigma^{\mathrm{R}}_{ij} &= C^{\mathrm{R}}_{ijkl}\left(\varepsilon^{\mathrm{I}}_{kl} + \varepsilon_{\infty kl} - \varepsilon^{(\mathrm{T})(\mathrm{R})}_{kl} + (z-h_0)\left(\kappa^{\mathrm{I}}_{kl} - \kappa_{\infty kl}\right)\right)
\end{aligned} \tag{32}$$

where

$$\begin{aligned}
\begin{Bmatrix} \varepsilon^{\mathrm{I}}_{ij} + \varepsilon_{\infty ij} \\ \kappa^{\mathrm{I}}_{ij} + \kappa_{\infty ij} \end{Bmatrix} &= \begin{bmatrix} A^{\mathrm{I}}_{ijkl} & B^{\mathrm{I}}_{ijkl} \\ B^{\mathrm{I}}_{ijkl} & D^{\mathrm{I}}_{ijkl} \end{bmatrix}^{-1} \begin{Bmatrix} N^{\mathrm{H}}_{kl} \\ M^{\mathrm{H}}_{kl} \end{Bmatrix} + \begin{Bmatrix} \varepsilon^{(\mathrm{init})(0)}_{ij} \\ \kappa^{(\mathrm{init})(0)}_{in} \end{Bmatrix} \quad \text{for } \mathbf{x} \notin \mathfrak{R} \\
\begin{Bmatrix} \varepsilon^{\mathrm{I}}_{ij} + \varepsilon_{\infty ij} \\ \kappa^{\mathrm{I}}_{ij} + \kappa_{\infty ij} \end{Bmatrix} &= \begin{bmatrix} A^{\mathrm{I}}_{ijkl} & B^{\mathrm{I}}_{ijkl} \\ B^{\mathrm{I}}_{ijkl} & D^{\mathrm{I}}_{ijkl} \end{bmatrix}^{-1} \begin{Bmatrix} N^{\mathrm{H}}_{kl} \\ M^{\mathrm{H}}_{kl} \end{Bmatrix} + \begin{Bmatrix} \varepsilon^{(\mathrm{init})(\mathrm{I})}_{ij} \\ \kappa^{(\mathrm{init})(\mathrm{I})}_{in} \end{Bmatrix} \quad \text{for } \mathbf{x} \in \mathfrak{R},
\end{aligned} \tag{33}$$

and perhaps only $\varepsilon^{(\mathrm{T})(\mathrm{R})}_{ij}$ is needed to be reminded as the initial strain prescribed in the patch associated with the thermal expansion coefficient mismatch, defined earlier in Eq. (12).

We conclude this section by a following remark. The development presented in Section 3.1 is quite similar to that given in Duong and Yu (2002a) for a stage II analysis of a plane stress problem. However, it includes the additional complexity associated with the out-of-plane bending. Moreover, it has been presented in a slightly different but better context.

3.2. Solution method for step 3 analysis

In step 3, an un-patched plate with an embedded grind-out cavity is considered, with strains and curvatures obtained from step 2 at the edges of the grind-out applied at infinity (see Fig. 2(c)). The analysis in this step can be carried out in a similar manner as in step 2 with the following minor changes. First, since an

un-patched plate is considered, the stiffness tensors of the inhomogeneity and the surrounding region will not include the patch's contribution. Second, as mentioned in Section 2, uniform strains and curvatures applied at infinity in the present problem are obtained from step 2 at the edge of the grind-out, not at the cavity center, and they are given by similar expression as Eqs. 10 and 11. However, since the reference plane at which the main plane strains are measured is chosen at $z = h_0$ in step 2 but at $z = t_p/2$ in step 3, in addition to the appropriate changes in the subscripts "plate's middle" in these two equations, the plus sign in Eq. (10) also must change to minus sign to account for this different choice of reference plane. Finally, since only an un-patched plate is considered in this step and the plate itself does not involve any initial strain (the initial strain field is only prescribed within the patch via Eq. (12)), all $N_{ij}^{(T)}$, $M_{ij}^{(T)}$, $\varepsilon_{ij}^{(init)(0)}$, $\kappa_{ij}^{(init)(0)}$, $\varepsilon_{ij}^{(init)(I)}$, $\kappa_{ij}^{(init)(I)}$, $\varepsilon_{ij}^{(init)(I\text{-}min)}$ and $\kappa_{ij}^{(init)(I\text{-}min)}$ must be set to zero in all formula derived in Section 3.1 as they are applied to the analysis of step 3.

It would be difficult to supply a precise error analysis for the present approximate method: its accuracy is most readily assessed by comparison with finite element results for particular cases. This is what is depicted in Section 4.

4. Numerical examples

To illustrate the present method, two examples corresponding to typical repair configurations are considered in this section. In the first example, an octagonal patch bonded over a circular grind-out cavity with a spherical depth as shown in Fig. 4 is analyzed. The material properties and thickness of the base plate and the patch are given below:

Base plate: Aluminum, $E = 72.4$ GPa, $v = 0.33$, $t_p = 5.08$ mm, $\alpha_p = 22.5.\text{E}{-}06/^\circ\text{C}$.

Patch: Boron/Epoxy, $E_x = 18.7$ GPa, $E_y = 193.6$ GPa, $v_{yx} = 0.21$, $G_{xy} = 5.5$ GPa, $t_R = 0.79$ mm, $\alpha_x = 21.4\text{E}{-}06/^\circ\text{C}$, $\alpha_y = 4.3\text{E}{-}06/^\circ\text{C}$.

The diameter and depth of the grind-out cavity are 25.4 and 2.54 mm (50% grind-out), respectively. Two different loading conditions are considered in this example. In the first loading condition, a stress

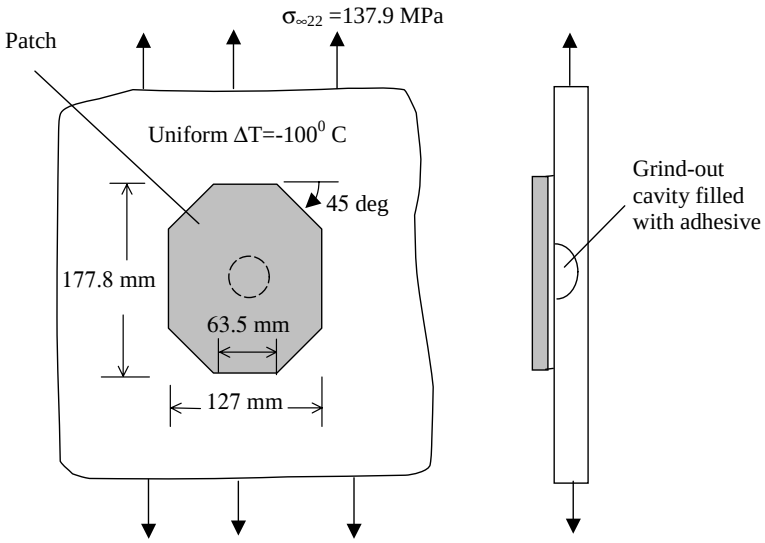

Fig. 4. Geometry of the example problem.

Table 1
Maximum stress concentration at the bottom of a grind-out cavity for different grind-out depths and different loading conditions

Loading	Grind-out depth (mm)	Maximum K_t at bottom of grind-out cavity	
		Analytical	FE
137.9 MPa	2.54	1.418	1.529
137.9 MPa and −100 °C	2.54	1.793	1.915
137.9 MPa	4.06	1.954	2.143
137.9 MPa and −100 °C	4.06	2.511	2.350

$\sigma_{\infty 22} = 137.9$ MPa is applied to the repaired plate at infinity. To address the effect of thermal stresses, in a second loading condition, a uniform temperature change of −100 °C is imposed on the repair in addition to the far field stress. On the other hand, the repair configuration of the second example is identical to the first example except for a deeper grind-out cavity (80% grind-out) with the plate's remaining thickness of 1.02 mm. Analytical predictions for the maximum stress concentration at the bottom of the grind-out cavity in the principal loading direction are summarized in Table 1. In all cases, the maximum stress concentration occurs at inner wall of the cavity as expected and it is normalized with respect to the far field applied stress of 137.9 MPa. For each repair configuration and loading condition, analyses corresponding to steps 1–3 were performed. The maximum stress in the plate at the bottom of the cavity were calculated using Eqs. (3)–(6) with the inner and outer wall fiber stresses computed from steps 2 and 3, and with the corresponding plane-stress type result (i.e., the one without considering the out-of-plane deflections) available in Duong and Yu (2002a). The plane stress results for these two problems are repeated in the last column of Table 2 for reference, and they are also compared with the present results there. It is clear from Table 2 that the use of these plane-stress type results for the prediction of the maximum K_t at the bottom of a cavity after one-sided patching in an unsupported structure will *not* be conservative. The present analyses yield a higher K_t at the bottom of the cavity since the cavity is either assumed to be unfilled or filled with a soft adhesive so that the cavity wall there tends to deflect toward the patch to align with the line of load, causing a linear stress distribution across the cavity wall thickness with a maximum value at the inner wall (a side adjacent to the adhesive). Illustration of this local out-of-plane deflection by the finite element analysis will be presented in the next paragraph.

To assess the accuracy of the analytical method, results from the 3-D finite element analyses are also obtained and compared with analytical predictions in Table 1. Finite element analyses are carried out using NASTRAN (solution 106, a geometrically nonlinear analysis). The adhesive is also modeled in the finite element analysis and the cavity assumes to be filled with the adhesive as in the actual repair. The shear modulus the adhesive and the bond line thickness are 0.46 GPa and 0.127 mm, respectively. The base plate, the adhesive and each ply of the patch are modeled by 8-node hexahedral solid elements. A very fine mesh is employed for regions inside and around a cavity to enable to model the spherical surface of the cavity with a great accuracy. In the FE model, the base plate is restrained from the out-of-plane deflection along its periphery. A typical mesh used in the FE analyses is given in Fig. 5. A typical deformation and stress

Table 2
Comparison of the maximum K_t between the present analyses and those from Duong and Yu (2002a)

Loading	Grind-out depth (mm)	Maximum K_t at bottom of grind-out cavity	
		Present analysis	Plane-stress type analysis (Duong and Yu, 2002a)
137.9 MPa	2.54	1.418	1.140
137.9 MPa and −100 °C	2.54	1.793	1.442
137.9 MPa	4.06	1.954	1.692
137.9 MPa and −100 °C	4.06	2.511	2.146

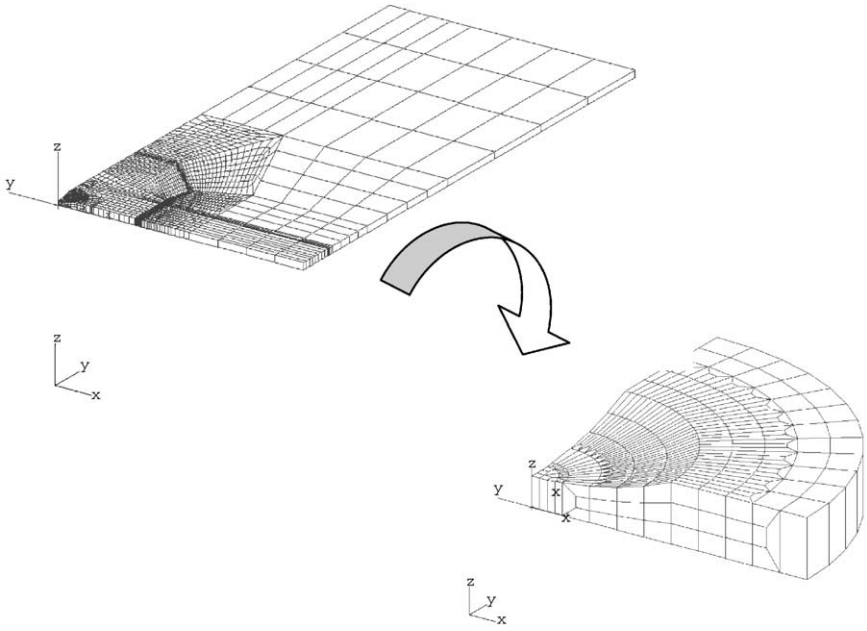

Fig. 5. A mesh of a damaged plate used in the FE analysis.

distribution across the wall thickness at the bottom of the cavity are illustrated in Figs. 6 and 7, respectively. These figures are obtained from the results of the case of 80% grind-out and with the thermal effect. Figs. 6 and 7 clearly indicate that the cavity wall near the bottom of the cavity deflects locally toward the patch, as mentioned in the preceding paragraph. From Table 1, the analytical predictions are in good agreement with the 3-D FE results. However, the minimum stress concentrations there (not reported here), particularly at outer wall of the cavity, are significantly higher than those obtained from the finite element method. Nevertheless, since only the maximum stress concentration at the bottom of the cavity is important

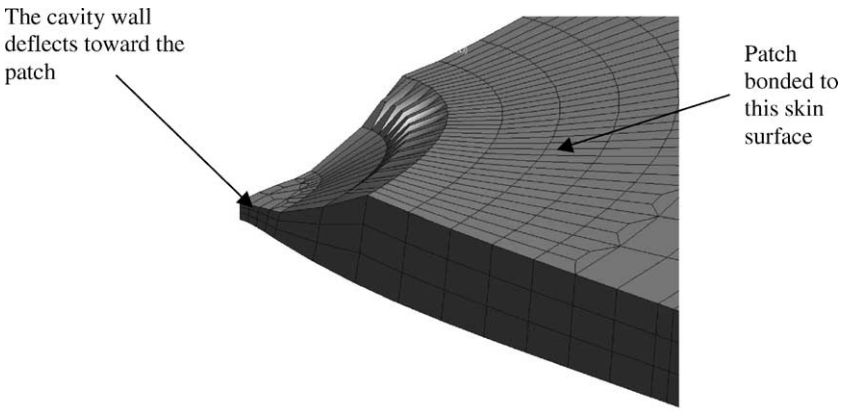

Fig. 6. Local deflection of a skin with an embedded cavity after one-sided patching. For clarity, the patch is not shown in the picture.

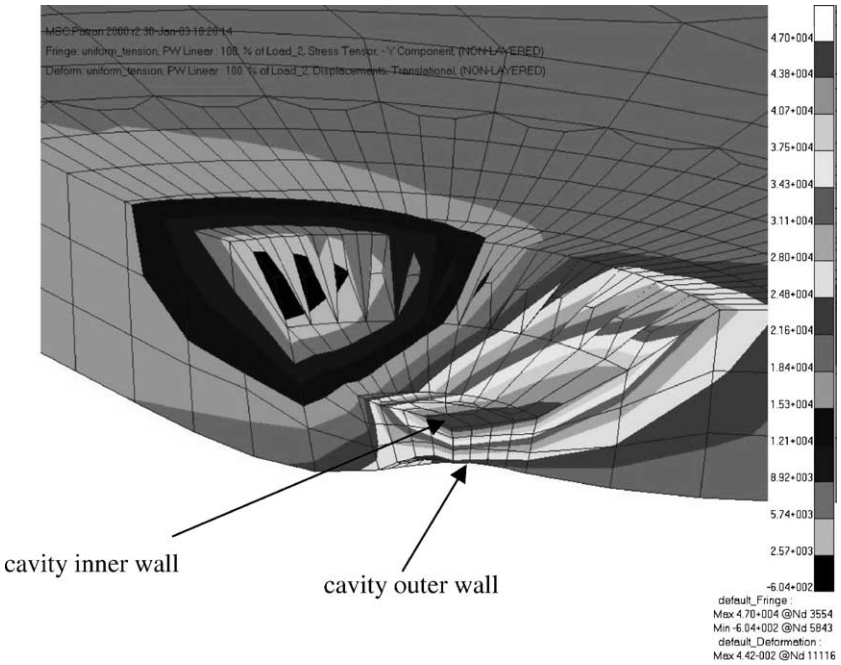

Fig. 7. Stress distribution across the cavity wall thickness with a maximum value at the inner wall (the side adjacent to the adhesive).

from the practical design viewpoint, no further improvement on the analytical model for these analyses is planned.

5. Conclusions

An analytical method to estimate the maximum stress concentration at the bottom of a grind-out cavity after one-sided patching is presented. The method is based on three steps analysis procedure. A good agreement is observed between the analytical predictions and the FE results for the maximum stress concentration at the bottom of the grind-out cavity. Unless the structure is well supported against the out-of-plane deflection, for example by stiffeners attached to one side of the structure, the out-of-plane bending due to the load path eccentricity causes stresses in the repaired skin near the bottom of the grind-out cavity vary significantly through a remaining skin's thickness with inner wall fiber stresses higher than the corresponding plane-stress type results. The prediction based on the plane-stress type analysis (i.e., one without considering the out-of-plane deflection) therefore may not be conservative in estimating the stress concentration at the bottom of the cavity after one-sided patching. The present paper extends the analytical capabilities for analysis/design of bonded repairs to the analysis of out-of-plane bending of a corrosion cavity reinforced with a composite patch.

Acknowledgements

The author takes this opportunity to gratefully acknowledge the support provided for this research by the USAF, WPAFB Ohio, as part of the CRAS (Composite Repair of Aircraft Structures) program under the management of Mr. David Stargel. The contract number is F33615-97C-3219.

References

Beom, H.G., Earmme, Y.Y., 1999. The elastic field of an elliptic cylindrical inclusion in a laminate with multiple isotropic layers. Journal of Applied Mechanics 66, 165–171.

Duong, C.N., Yu, J., 2002a. Stress analysis of a bonded repair over a corrosion grind-out using an inclusion model with a second ordered eigenstrain theory. International Journal of Engineering Science 40, 347–365.

Duong, C.N., Yu, J., 2002b. Analysis of a plate containing a polygon-shape inclusion with a uniform eigencurvature. Journal of Applied Mechanics, in press.

Duong, C.N., Yu, J., 2002c. An engineering approach to geometrically nonlinear analyses of a one-sided composite repair under thermo-mechanical loading. Theoretical and Applied Fracture Mechanics, submitted for publication.

Duong, C.N., Hart-Smith, L.J., Yu, J., 2001a. Analytical approach to bonded repair of elliptical dent, corrosion grind-out and cut-out. Theoretical and Applied Fracture Mechanics 36, 187–193.

Duong, C.N., Wang, J.J., Yu, J., 2001b. An approximate algorithmic solution for the elastic fields in bonded patched sheets. International Journal of Solids and Structures 38, 4685–4699.

Hart-Smith, L.J., 2002. Analyses of adhesive peel and shear stresses in bonded single-strap joints and one-sided patches and doublers. Accounting for Thermal Mismatch Effects, in preparation.

Jones, R.M., 1975. Mechanics of Composite Materials. McGraw-Hill, New York.

Mura, T., 1987. Mechanics of Defects in Solids. Martinus Nijhoff, The Hague.

Rodin, G.J., 1996. Eshelby's inclusion problem for polygons and polyhedra. Journal of Mechanics and Physics of Solids 44, 1977–1995.

Rose, L.R.F., 1988. Theoretical analysis of crack patching. In: Baker, A.A., Jones, R. (Eds.), Bonded Repair of Aircraft Structures. Martinus Nijhoff, The Hague.

Wang, C.H., Rose, L.R.F., 1999. A crack bridging model for bonded plates subjected to tension and bending. International Journal of Solids and Structures 36, 1985–2014.